

# Critical adsorption of polyelectrolytes onto charged Janus nanospheres

Sidney J. de Carvalho,<sup>1</sup> Ralf Metzler,<sup>2,3</sup> and Andrey G. Cherstvy<sup>2</sup>

<sup>1</sup>*Department of Physics, São Paulo State University, São Paulo, Brazil*

<sup>2</sup>*Institute for Physics and Astronomy, University of Potsdam, Potsdam-Golm, Germany*

<sup>3</sup>*Department of Physics, Tampere University of Technology, 33101 Tampere, Finland*

Based on extensive Monte Carlo simulations and analytical considerations we study the electrostatically driven adsorption of flexible polyelectrolyte chains onto charged Janus nanospheres. These net-neutral colloids are composed of two equally but oppositely charged hemispheres. The critical binding conditions for polyelectrolyte chains are analysed as function of the radius of the Janus particle and its surface charge density, as well as the salt concentration in the ambient solution. Specifically for the adsorption of finite-length polyelectrolyte chains onto Janus nanoparticles, we demonstrate that the critical adsorption conditions drastically differ when the size of the Janus particle or the screening length of the electrolyte are varied. We compare the scaling laws obtained for the adsorption-desorption threshold to the known results for uniformly charged spherical particles, observing significant disparities. We also contrast the changes to the polyelectrolyte chain conformations and the binding energy distributions close to the adsorption-desorption transition for Janus nanoparticles to those for simple spherical particles. Finally, we discuss experimentally relevant physico-chemical systems for which our simulations results may become important. In particular, we observe similar trends with polyelectrolyte complexation with oppositely but heterogeneously charged proteins.

Abbreviations: ES, electrostatic; PE, polyelectrolyte; JNS, Janus nanosphere; WKB, Wentzel-Kramers-Brillouin.

## I. INTRODUCTION

Janus grains [1] or particles of spherical, cylindrical, or disc-like architecture are nanoparticles whose surface is divided into two or more areas with distinct physico-chemical properties. For instance, the behaviour of Janus particles with one apolar hydrophobic half and a polar or charged half [2] share common features with surfactant assembly in solutions [3]. Charged Janus nanospheres (JNSs), our main focus in this study, exhibit two oppositely charged hemispheres. We study in detail the critical adsorption conditions for a polyelectrolyte chain, see Fig. 1. From extensive Monte Carlo simulations as well as analytical calculations we demonstrate that the adsorption behaviour to JNS significantly differs from that to homogeneously charged spheres. The polyelectrolyte adsorption is investigated with respect to changes in the size of JNSs and salinity of the electrolyte.

Janus particles have become widely used model systems. Thus, orientation-sensitive interactions between JNSs [4] are extensively used in directed supra-molecular hierarchical assembly [5, 6]. Janus particles are promising candidates for designing novel materials, responsive sensor nano-devices, biomedical and pharmaceutical applications, anti-reflection coatings, stabilising liquid-liquid interfaces, as well as nanoscale chemical locomotion [2, 7–9]. “Hairy” Janus particles decorated via grafting [10] of various polymers [8] reveal rich stimuli-responsive behaviour [11] and can serve as coatings of immiscible liquid-liquid interfaces [12, 13].

The weak and strong adsorption of polyelectrolytes (PEs) onto oppositely charged interfaces has a number of important technological and biological applications [14].

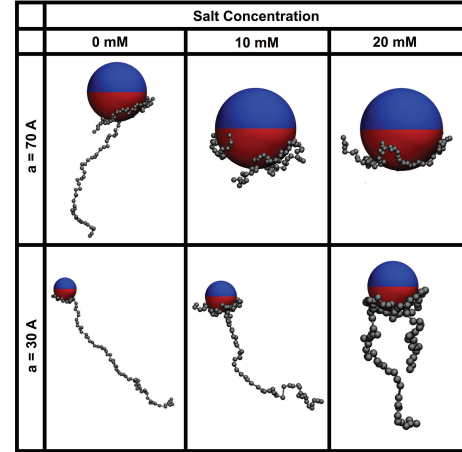


Figure 1: Typical conformations of PE chains in front of JNS of radii  $a = 70 \text{ \AA}$  (top) and  $a = 30 \text{ \AA}$  (bottom), as obtained from our computer simulations (particles are shown not to scale). The salt concentration from left to right is 0, 10, and 20 mM and the particle surface charge density is  $\sigma a^2 \approx 7.5$ .

These include, inter alia, paper production, various surface coating techniques, colloid stabilisation, adsorption of nucleic acids on the interior of viral shells, DNA wrapping in nucleosomes, pharmacological applications, etc. Of particular interest is the regime of weak adsorption, referring to weakly charged PEs below the Manning’s counterion condensation limit [15, 16], i.e., charge-charge distances along the PE contour are shorter than the Bjerrum length  $l_B$ . A fundamental feature of weak PE adsorption is the transition between the entropically driven free state of the PE chain in solution and the bound state

close to the interface. The latter is favoured by electrostatic (ES) PE-surface attractions, which are typically screened exponentially by the surrounding electrolyte in a Debye-Hückel fashion. This transition defines the condition for the *critical adsorption* of PE chains, at which the entropic penalty of PE confinement near the interface is exactly balanced by the energetic attraction to the surface. At larger electrolyte salinities the PE-surface attractions are better screened and thus larger surface charge densities are necessary to trigger the adsorption. The study of this transition for dipolar JNSs is the main target of the present study, as depicted in Fig. 1.

Theoretically, the adsorption of PE chains onto uniformly charged surfaces was studied to great detail, see, e.g., Refs. [14, 17–31]. The regime of weak PE-surface adsorption for which the entropy of the PE chain is still important, was extensively studied by computer simulations [32–44]. The characteristics of the PE-surface adsorption including the conditions for the critical adsorption of long PE chains with a constant linear charge density onto planar [45, 46] and curved [14, 47–58] interfaces were also derived. Apart from the more conventional strong PEs, the adsorption of weak charge-regulated PEs and poly-ampholyte chains onto spherical particles was investigated by computer simulations [59–61] as well as experiment [62, 63].

The paper is organised as follows. In Sec. II we set the scene by briefly reviewing the main results for the critical PE adsorption onto planar and curved surfaces. Sec. III elucidates the PE adsorption onto JNSs and discusses the core results of the current paper obtained from extensive Metropolis Monte-Carlo computer simulations. We vary the solution salinity, the particle radius, and the length of polymer chains to unveil their impact on the location of the adsorption-desorption boundary. In Sec. V we discuss our results, outline their possible applications, and draw our conclusions. App. A details the exact solution of the ES potential around a JNS within the linear Poisson-Boltzmann model. In App. B the equations for the 2D WKB theory of PE adsorption are derived.

## II. CRITICAL POLYELECTROLYTE ADSORPTION

We here briefly review the results for the critical PE adsorption onto planar and curved interfaces necessary for our discussion regarding PE-JNS adsorption below. The PE adsorption occurs when the gain of the PE-surface ES attraction becomes larger than the free energy loss due to the decrease in the conformational entropy of the adsorbed PE chain. Critical adsorption conditions relate the surface charge density  $\sigma$ , the PE linear charge density  $\rho$ , the ambient temperature  $T$ , the persistence length  $b/2$  of the PE chain, the radius of curvature  $a$  of the surface, and the electrolyte concentration. These quantities are connected by the single universal adsorption parameter, denoted below as  $\delta$ . The precise form of this coupling is

[53]

$$\delta_c = 24\pi \frac{|\sigma_c \rho|}{\epsilon k_B T b} a^3, \quad (1)$$

where the subscript  $c$  denotes the value at the critical adsorption point.

The exact value of  $\delta_c$  decides whether for given physical parameters a PE chain adsorbs onto the surface or stays unbound. In the particular case of a *planar* interface the exact analytical result for long flexible PE chains shows that the critical surface charge density  $\sigma_c$  scales with the third power of the reciprocal Debye screening length  $\kappa = 1/\lambda_D$  [45], so that the approximate result is

$$\delta_c^{pl}(\kappa) \approx 1.45 (\kappa a)^3. \quad (2)$$

This result is getting modified substantially for more complex surface geometries and its physical properties. For instance, larger plane surface charge densities are necessary to induce PE adsorption when the surface is low-dielectric [56]. Due to PE-PE image-force repulsion [24] in the course of adsorption, substantially larger critical strengths  $\delta_c$  are required to trigger polymer adsorption. In addition, in the low-salt limit the cubic scaling  $\delta_c \sim \sigma_c \sim \kappa^3$  given by expression (2) is modified to the quadratic scaling  $\delta_c \sim \kappa^2$  [56].

For *curved* convex surfaces, higher values of  $\sigma$  are necessary to activate the adsorption, as a larger entropic penalty needs to be paid for the polymer confinement near the surface, meaning that the value of  $\delta_c$  becomes larger than  $\delta_c^{pl}$ . Moreover, the scaling  $\delta_c(\kappa)$  changes with the surface curvature and the salinity of the electrolyte. These two quantities can be combined into a dimensionless parameter  $\kappa a$  controlling the scaling behaviour  $\delta_c(\kappa a)$  for long chains. Specifically, in the limit of low salt or large surface curvature, when  $\kappa a \ll 1$ , it was shown recently that for a *spherical particle* the linear dependence

$$\delta_c^{sp}(\kappa) \approx 0.90 (\kappa a)^1. \quad (3)$$

emerges [53]. For otherwise given parameters, this relation determines the minimal sphere radius  $a_c$  required for PE adsorption as well as the critical adsorption temperature  $T_c$ . For flexible PEs in front of a *cylindrical interface* the scaling relation becomes

$$\delta_c^{cyl}(\kappa) \approx 1.07 (\kappa a)^2 \quad (4)$$

in the limit  $\kappa a \ll 1$  [53]. This change in the exponent for spherical versus cylindrical particles is corroborated by experimental data [64] (see also Fig. 11 and the discussion in Ref. [51]).

To derive the scaling relations (3) and (4), the Wentzel-Kramers-Brillouin (WKB) approximation scheme known from quantum mechanics was employed [53]. It accurately reproduces the known results, including the prefactors, for  $\delta_c(\kappa a)$  in planar [45] and spherical [50] geometries. In the opposite limit of  $\kappa a \gg 1$  the WKB theory predicts that for convex surfaces  $\sigma_c$  approaches the

value for the uniformly charged plane from above, and the scaling (2) is valid [53]. The reasons for this are a) the sphere and cylinder ES potentials are lower than the one for the planar surface with identical  $\sigma$  and b) the polymer conformations are perturbed more strongly on adsorption onto convex surface-limited interfaces such as those of spherical and cylindrical particles. This reduction of the number of polymer translational degrees of freedom requires larger  $\sigma_c$ , particularly at low salinities and small  $\kappa a$  values. Concurrently, in the low-salt limit a systematic change in the scaling of the critical adsorption parameter  $\delta_c$  was predicted [53], in qualitative agreement with experimental observations [63], see Sec. V. Extensive comparison of theoretical predictions for the critical PE adsorption onto spherical versus cylindrical surfaces to a number of experimental data sets was presented in Refs. [14, 51].

These theoretical predictions for critical PE adsorption were corroborated indirectly by experiments, in that complex formation and coacervation of PEs with oppositely charged particles revealed no adsorption and agglomeration for  $\kappa$  above the critical value, when strong screening effects significantly reduce the PE-particle ES attraction [62–70]. The critical surface charge density  $\sigma_c \sim \kappa^\nu$  for spherical and cylindrical particles was demonstrated to increase with  $\kappa$  as follows [70]

$$\sigma_c^{sp}(\kappa) \sim \kappa^{1\dots 1.8} \text{ and } \sigma_c^{cyl}(\kappa) \sim \kappa^{1.8\dots 2.5}. \quad (5)$$

The scaling exponents  $\nu$ , being sensitive functions of PE stiffness and linear charge density, clearly differ from the cubic dependence (2) due to curvature effects of adsorbing interfaces as well as the finite available adsorption surface and salt-dependence of PE persistence length  $l_p$ .

These critical adsorption results for uniformly charged interfaces have to be modified in many realistic situations when quenched or annealed charge patterns exist on the adsorbing surfaces. This may be due to the discrete nature of surface charges or some inherent non-uniform or rough structure of interfaces. For *planar patterned* surfaces, several theoretical [71, 72] and in silico [73–76] studies are available which focused on the effects of charge inhomogeneities on PE adsorption. For instance, for a circular charged patch of radius  $R$  the critical PE adsorption condition was derived in a variational model [73]. As expected, a patch of a finite size demands higher  $\sigma$  values to enable adsorption [73, 77]. Effects of the patch size and charge distribution for polyion-protein complexation were analysed by computer simulations for complexes close to the isoelectric point [78], see also Ref. [79]. Computer simulations for planar patterned charged interfaces were also reported [72].

For *curved patterned* interfaces, however, the understanding of the critical PE adsorption remains elusive. It is the main purpose of the present study to advance the knowledge on this process. We focus on PE adsorption onto JNS depicted in Fig. 1 which is the ultimate example of a net-neutral patchy colloid [2]. It consists of two equally but oppositely charged hemispheres so that

the area of charged patches and surface curvature are intimately coupled. We show that this surface charge distribution effects a non-trivial interplay of the patch-size-mediated adsorption-desorption and the particle size, adds interesting new insight to the theory of PE adsorption onto curved interfaces, and represents a first step towards a more general approach to less orderly charge distributions.

In what follows we use Metropolis Monte-Carlo computer simulations to quantify the conditions of the critical PE adsorption as a function of the surface charge density and curvature of JNSs, the salinity of the solution, and the length of PE chains. The simulations are based on an algorithm, which was previously successfully implemented by one of the author to study the PE adsorption onto spherical and cylindrical uniformly-charged interfaces [44, 57].

### III. SIMULATIONS OF PE-JNS ADSORPTION

#### A. Specification of the model and the employed parameters

A single JNS of radius  $a$  is fixed at the centre of a spherical simulations box containing a single PE chain. The latter is modelled as a bead-spring polymer consisting of  $N$  single-charged spherical monomers connected by harmonic elastic potentials

$$E_{el}(\delta r_{i,j}) = \frac{1}{2} k r_{i,j}^2, \quad (6)$$

and interact via the screened Coulomb ES potential with a hard-core restriction,

$$E_{ES}(r_{i,j}) = e_0^2 \frac{\exp(-\kappa r_{i,j})}{\epsilon r_{i,j}}. \quad (7)$$

Here  $r_{i,j}$  is the distance between monomers  $i$  and  $j$  with  $1 > (i, j) > N$  and  $i \neq j$ , and we set  $e_0 = 1$  below. This inter-monomer ES repulsion yields a *finite* persistence length of the polymer that will be a crucial ingredient for the critical adsorption conditions derived in Sec. IV C. We thus explicitly account for the intra-chain charge-charge interactions for finite-length chains, a situation which would require a formidable theoretical modelling. The chain parameters are the same as used in Ref. [44] to study the PE-cylinder adsorption. The screened monomer-monomer interactions imply a finite PE ES persistence length,  $l_p^{el}$ , in contrast to the ideal Gaussian chains often employed in theoretical approaches [53].

The ES interactions of the  $i$ th PE monomer with the JNS is governed by the attractive dipolar-like potential  $\Psi_J$  given by Eq. (A3) in the Appendix, see also Fig. 2 for the ES potential distribution. PE-JNS ES binding energy then is

$$E_B(r_i, \theta_i) = e_0 \Psi_J(r_i, \theta_i). \quad (8)$$

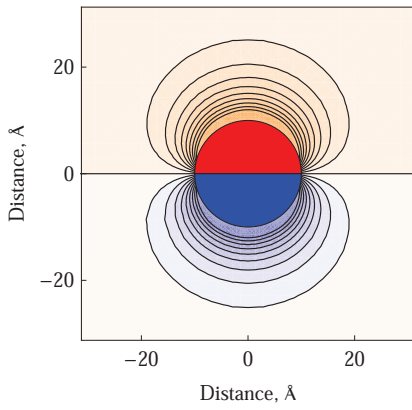


Figure 2: Two-dimensional contour-plot of the ES potential  $\Psi_J(r, \theta)$  around the JNS as given by Eq. (A3). Blue represents the positive and red the negative values of the potential. Parameters:  $a = 10 \text{ Å}$ ,  $1/\kappa = 10 \text{ Å}$ , and  $S_0 = 300 \text{ Å}^2$ .

Simulating the PE adsorption onto a uniformly charged sphere, Eq. (A5) for  $\Psi_{sp}(r)$  is used. The aqueous solution has the standard dielectric constant  $\epsilon = 78.7$  and temperature  $T = 298.15\text{K}$ . The monomer radius is  $r = 2 \text{ Å}$ , and each monomer carries the elementary charge  $e_0$ . The system is confined inside a large electrically-neutral simulations cell to eliminate end- and finite-size effects.

To sample the polymer configurations, translational movements of individual monomers and of the whole chain are combined with the Pivot rotation, see the detailed description in Ref. [44]. A Metropolis Monte-Carlo approach in the canonical ensemble is implemented to explore the configurations space of the polymer-particle system. The standard Weighted Histogram Analysis Method (WHAM) is used to compute the system free energy. The polymer profiles are computed from the distribution functions of its monomers and their centre-of-mass  $\mathbf{R}_{CM}(t)$  generated, as a function of the distance from the macro-ion surface of JNSs,  $p(\mathbf{R}_{CM} - \mathbf{R}_m)$ .

### B. Adsorption criterion

The criterion for the PE-particle adsorption is based on the following considerations. As we observed for the interaction of a PE chain with a uniformly charged sphere, at higher ionic strengths the particle-PE attraction cannot overcome the loss of conformational and translational polymer entropy, and thus no adsorption takes place [57]. With a decreasing salinity, a *discontinuous*, first-order transition between the adsorbed and desorbed states of the PE chain occurs. The adsorbed state is characterised by binding energies of, typically, several units of the thermal energy  $k_B T$ , whereas the desorbed state has zero energy. This “gap” allows us to count the fraction of polymer configurations generated from simulations in each state, without defining an (arbitrary) energy threshold or a shell around the adsorbing particle

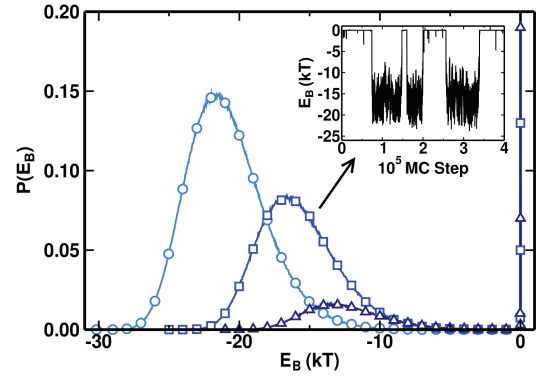


Figure 3: Distribution  $p(E_B)$  of the ES binding energy obtained from simulations of PE-JNS adsorption at varying salinities. The inset shows the temporal evolution of the binding energy  $E_B(t)$ , tracing transitions between the adsorbed and desorbed states of the PE chain, in units of the thermal energy  $k_B T$ . The profiles are normalised to unity when the zero binding energy contributions stemming from the desorbed states (shown as vertical lines at  $E_B = 0$ ) are considered as well. Parameters: the JNS surface charge density is  $\sigma = 25\text{mC/m}^2$  (bluish colours for the curves), salt concentration is 20 (circles), 30 (squares) and 40 mM (triangles), the JNS radius is  $a = 70 \text{ Å}$ , and the number of PE monomers is  $N = 20$ .

to distinguish adsorbed versus desorbed PE monomers. Following this observation, we count the polymer as adsorbed if more than 50% of the configurations are in the adsorbed state during the simulation time. Typically of the order of  $10^6$  to  $10^7$  polymer configurations are used for averaging. As we show below, for PE-JNS adsorption there exists indeed a similar critical energetic transition between the adsorbed and desorbed states.

## IV. MAIN RESULTS

### A. Binding energies and distributions of PE monomers

Typical conformations of the PE chain in the proximity of JNSs of different sizes and at varying salinity of the solution are presented in Fig. 1. The differences for varying conditions are striking, ranging from a completely adsorbed chain to a configuration, in which the chain is marginally attached to the JNS and points almost completely straight away from it. We observe that at higher salinities and larger Janus spheres a more pronounced PE adsorption takes place. This trend with the solution salinity is opposite to that for PE-sphere adsorption, where the adsorption gets amplified in low-salt conditions. For PE-JNS adsorption at low salt, the ES PE attraction by the oppositely charged hemisphere is accompanied and compensated by ES repulsion by the similarly charged Janus hemisphere, reducing the num-

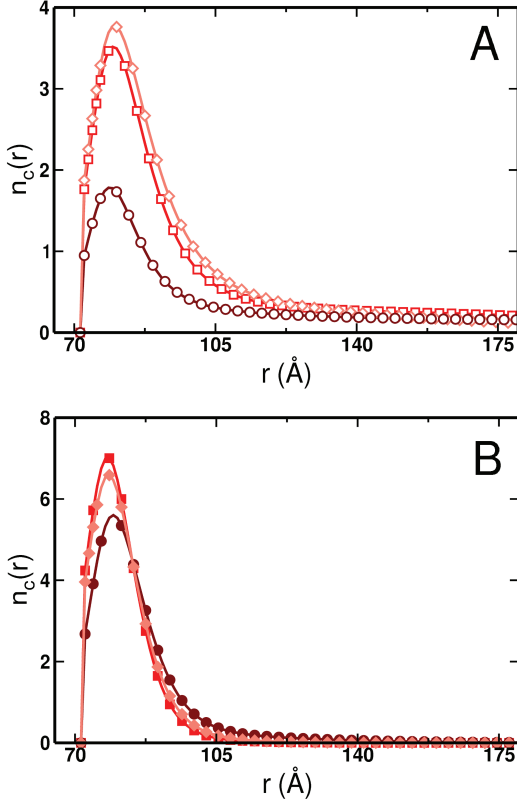


Figure 4: Number of adsorbed PE monomers  $n_c(r)$  versus distance from the adsorbing JNS (panel A, open symbols) and from the uniformly charged sphere (panel B, filled symbols). Parameters:  $\sigma = 12.5$  mC/m<sup>2</sup> (reddish colours for the curves), salt concentration is 0 (circles), 6 (squares) and 14 mM (rhombi),  $a = 70$  Å, and  $N = 100$ .

ber of polymer monomers adsorbed onto the JNS surface as  $\kappa$  decreases, see Fig. 4A.

As illustrated in Fig. 3, there occur pronounced changes of the binding energy when transitions between the PE adsorbed and desorbed states in the vicinity of the JNS occur. More specifically, the inset of Fig. 3 shows the time trace of the PE-JNS binding energy  $E_B(t)$  in a given simulations run, while the main panel of Fig. 3 illustrates the long-time equilibrium probability distribution  $p(E_B)$  of the adsorption energy  $E_B$ . We observe that PE chains at progressively higher salt concentrations have, as expected, smaller magnitudes  $|E_B|$  of ES attraction to the JNS, see the differences between the circles, squares, and triangles in Fig. 3, for increasing salinity. At low salt each PE monomer in the bound state has a binding energy of about one unit of the thermal energy  $k_B T$ , which corresponds to the ratio of the  $E_B$  values of Fig. 3 versus the number of monomers,  $N = 20$ . The distributions  $p(E_B)$  are normalised to unity when the contributions of both adsorbed and desorbed PE states, with zero binding energy, are accounted for. The latter are represented by the vertical lines at  $E_B = 0$  in Fig. 3. As expected, at lower salt and thus stronger ES attraction, the proportion of

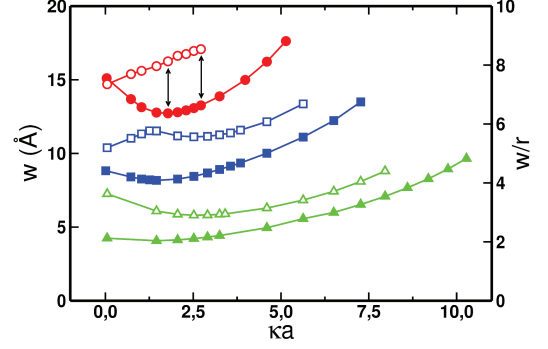


Figure 5: Dependence of the width of the layer of the adsorbed PE monomers at the JNS surface (open symbols) and the surface of a uniformly charged sphere (filled symbols) versus the salinity of the electrolyte solution. Parameters:  $\sigma = 12.5$  (red circles), 25 (blue squares), and 50 mC/m<sup>2</sup> (green triangles). We use a constant JNS radius  $a = 70$  Å and PEs with  $N = 100$  monomers. Approximately  $10^6$  polymer conformations were used in the averaging. The arrows show the salinities for the PE profiles presented in Fig. 4.

bound PE states increases, as given by the relative area under the distributions  $p(E_B < 0)$  in Fig. 3.

In Fig. 4 we show the non-normalised radial distribution function of the chain monomers facing the JNS (panel A) and a uniformly charged sphere with the same  $\sigma$  (panel B). We obtain a systematically broader distribution of monomers in front of the JNS compared to the sphere, consistent with the behaviour of the surface layer width, as shown in Fig. 5. With addition of salt, the profiles of PE chains adsorbed onto JNSs become progressively broader, as intuitively expected, and also more monomers are getting adsorbed, as illustrated in Fig. 4A.

Note that the PE monomer profiles in Fig. 4 are shown for the parameters well above the critical adsorption point. At the critical point itself, when  $\sigma \rightarrow \sigma_c$ , the width  $w$  of the polymer distribution diverges. For large surface charge densities, in contrast, the relation  $w(\sigma) \sim \sigma^{-\gamma}$  with  $\gamma \approx 1/3$  is valid, as shown for PE chains adsorbed onto planar and curved interfaces in Refs. [14, 53].

## B. Adsorbed layer width $w$

From Fig. 4 we obtain the width  $w$  of the adsorbed PE layer at the half-height of the monomer density profile  $n_c(r)$ . The width typically decreases for decreasing salinity, as shown in Fig. 5. This decrease occurs because of the stronger ES PE-particle attraction, both for PEs in the proximity of the JNS and the uniformly charged sphere (apart from a region of small values of  $\kappa a$ ). For the same physical reason, the PE layer width  $w$  decreases with  $\sigma$ , compare the curves with the open symbols in

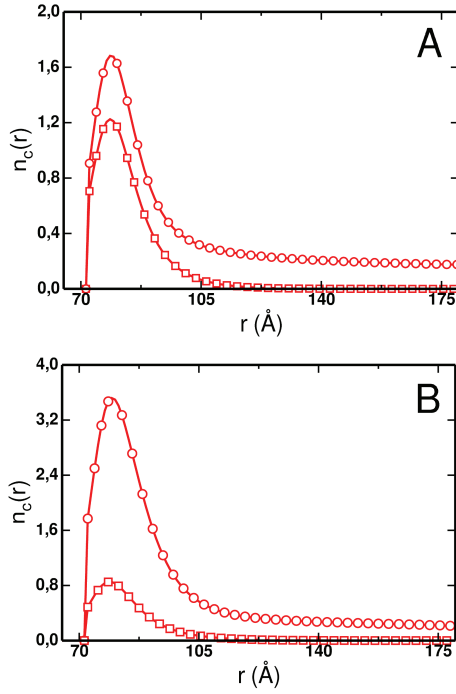


Figure 6: Radial distributions of PE monomers in front of JNSs at  $\sigma = 12.5 \text{ mC/m}^2$  (reddish colors) and salt concentration of 0 (panel A) and 6 mM (panel B). Other parameters are:  $N = 100$  (open circles) and  $N = 20$  polymer monomers (open squares), and JNS radius is  $a = 70 \text{ Å}$ .

Fig. 5.

The highest  $\kappa$  values in the curves of Fig. 5 correspond to the largest salinity of the solution at which PE-particle adsorption occurs (critical point). At even larger salt concentrations we have two distinct monomer populations: one of them is for PE chains staying near the particle corresponding to the adsorbed state, while another one is for PE monomers away from the Janus particle (the desorbed state). The range of salinities in terms of  $\kappa a$  in which the PE-JNS adsorption occurs is systematically *smaller* than that for the uniformly charged sphere, compare the open and filled symbols in Fig. 5. As expected, the PEs in front of the JNS give rise to somewhat *thicker* adsorption layers as compared to the PE adsorption onto the homogeneous sphere at the same conditions, as shown in Fig. 5. Another expected observation is the fact that for smaller values of Janus particle charge density  $\sigma$ , the region of  $(\kappa a)$  values of PE-JNS adsorption shrinks and shifts towards smaller  $\kappa a$  values. Therefore, for weakly charged JNSs even moderate salt conditions can prevent PE adsorption.

We also find that for shorter PEs experiencing weaker attraction to JNSs, the width  $w$  of the adsorbed PE layer for the surface charge densities given in Fig. 5 decreases, cf. Fig. 6. Physically, longer polymers do experience a stronger ES attraction and their monomers adsorb onto the JNSs in larger numbers. Because of a

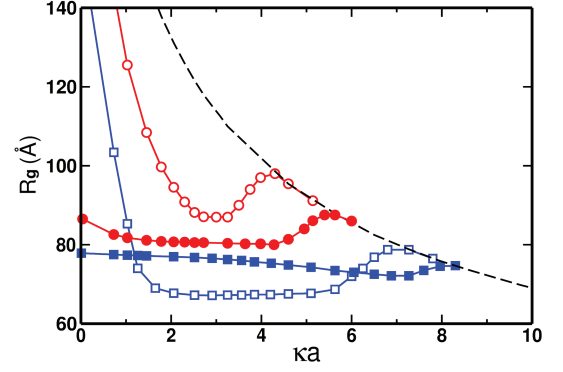


Figure 7: Radius of gyration of the PE chain adsorbed onto a uniformly-charged sphere (filled symbols) and a JNS (open symbols). Parameters, symbol notations, and colour scheme are the same as in Fig. 5 ( $a = 70 \text{ Å}$  and  $\kappa$  is varied). The dashed black curve indicates the size of a free semiflexible polymer with the proper  $l_p$  in solution.

limited nanoparticle surface available to PE deposition, however, longer PE chains crowd near the attractive JNS hemisphere. The chains therefore swell because of inter-monomer ES repulsion. All this gives rise to larger thicknesses of the adsorbed PE layer as  $N$  grows, see Fig. 6 for two values of the solution salinities.

We note that, unlike the planar and cylindrical cases for which the available surface for PE adsorption is infinite, for spheres and JNSs it is strictly bounded. This effects the extensive polymer *tail formation*, seen also in the sample configurations in Fig. 1. For this reason, the number of monomers in the adsorbed layer at the JNS surface changes with the ionic strength, resulting in the complex behaviour presented in Fig. 5.

Finally, in particular for strongly charged JNS, corresponding to the green triangles in Fig. 5, we observe a non-monotonic dependence of the adsorbed layer width on the salt concentration. This is indicative of a weaker ES attraction of PE chains to the JNS at low salt conditions, when the effects of the similarly charged JNS hemisphere is amplified, compensating the PE attraction to the similarly-charged JNS hemisphere. We refer also to Ref. [58] which investigates non-monotonic effects of added salt and non-electrostatic PE-surface interactions analytically and by simulations.

The variation of the radius of gyration  $R_g$  of the PE chain during the adsorption onto JNSs and the uniformly charged spheres is shown in Fig. 7. The slightly non-monotonic variation observed in this plot is quite sensitive to the system parameters, such as the particle size, its surface charge density, and the polymer length. The universal feature we want to highlight here, however, is the general dependence of  $R_g$  on the salt concentration. In particular, for salinities above the critical adsorption transition, the chain size follows the prediction for the non-confined semiflexible polymer in solution, both for



the JNS and the uniformly charged sphere, as shown by the dashed curve in Fig. 7. For very low salt concentrations, in contrast, the gyration radius of PE chains in front of the JNS starts to grow dramatically as the salinities drops below the critical salinity required for PE-JNS adsorption. This is indicative of stronger ES repulsion of PE chains from the similarly-charged JNS hemisphere. This repulsion is long-ranged in the low-salt limit and has a tendency to displace the polymer from the favorable JNS hemisphere as well as to stretch the chain. This stretching effect is shown on the left panel of Fig. 1 for vanishing salinity.

### C. Critical PE adsorption conditions

With our above adsorption criterion, we determine the critical adsorption conditions for PE chains of different lengths and JNSs of varying sizes. Our main conclusion is that there exists *no* universal scaling of the parameter  $\kappa a$  for PE adsorption onto JNSs, in strong contrast to the case for PE adsorption onto spherical and cylindrical interfaces [53]. The curvature of the JNS surface and the screening parameter  $\kappa$  cannot now be varied inter-changeably. The solution salinity and the surface curvature affect the dependence of the critical adsorption conditions in a disparate way. This is likely due to the salt effects on the PE persistence length  $l_p$ , see Fig. 8. Note that the range of  $\kappa a$  we present in Fig. 8 spans more than two decades, that is significantly more than examined recently for the PE-cylinder adsorption [44].

Let us now describe the *main results* of the current study presented in Figs. 8A and 8B. We start with the results for the uniformly charged sphere and consider a varying sphere radius  $a$ , the filled squares in Fig. 8B. We find the scaling  $\sigma_c \sim (\kappa a)^{2.7}$  in the limit of large  $\kappa a$ , in agreement with the limit of large spheres discussed in Ref. [53] or with the nearly planar result of Ref. [45] given by Eq. (2). In the limit of  $\kappa a \ll 1$  we observe that  $\sigma_c \sim (\kappa a)^1$ , in agreement with previous results for small spheres derived in Refs. [14, 50, 53] and described by Eq. (3). Note that from the results obtained for the critical surface charge density  $\sigma_c$  and the definition (1) one can recalculate the critical minimal radius  $a_c$  of the JNS particle necessary for adsorption.

#### 1. Varying Janus particle size

For JNSs of varying sizes at constant  $\kappa$ , we detect a similar turnover of the scaling behaviour  $\sigma_c(\kappa a)$ . The critical JNS surface charge density  $\sigma_c$  required to trigger the PE adsorption is *larger* than that for the uniformly charged sphere in the whole range of  $\kappa a$ , see the empty and filled symbols in Fig. 8B. The  $(\kappa a)$  region in which the change in the scaling behaviour for JNSs from  $\sigma_c \sim (\kappa a)^1$  to  $\sigma_c \sim (\kappa a)^\nu$  with  $\nu \approx 3$  occurs, is somewhat

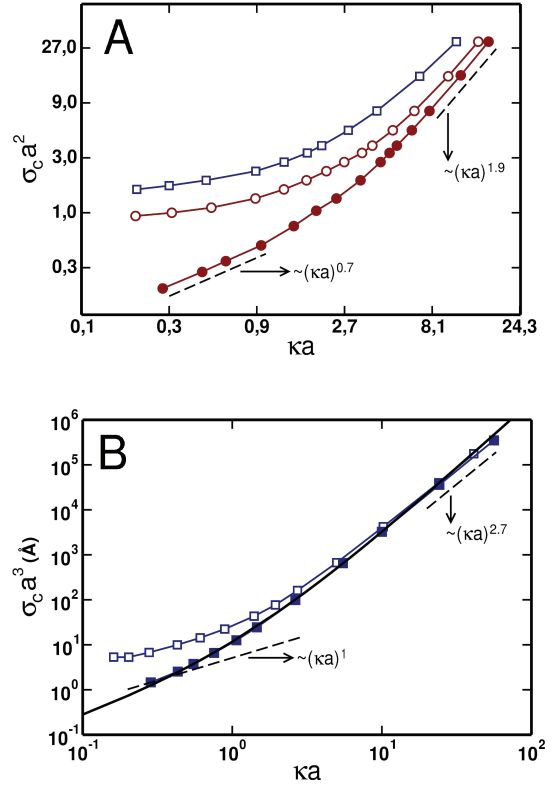


Figure 8: A: Variation of salinity. Results of computer simulations for the critical surface charge density  $\sigma_c$  of a JNS-particle for varying  $\kappa$ . Parameters: the constant JNS radius  $a = 70$  Å,  $N = 20$  chain monomers (open squares),  $N = 100$  (open circles). The results of the same simulations method for a uniformly charged sphere are shown as filled circles (polymer length is  $N = 100$ ). B: Variation of the Janus particle radius. The adsorption-desorption threshold at  $\approx 50$  mM of 1:1 salt ( $\lambda_D \approx 13.6$  Å) and polymer length  $N = 20$  (open squares) at varying JNS radius  $a$ . The results for PE chains with  $N = 20$  monomers in the proximity of a uniformly charged sphere are represented by the filled squares. The theoretical asymptote of Ref. [53] for PE-sphere adsorption given by Eq. (B5) multiplied by 1.77 is shown as the solid black curve. On a standard 3-3.5 GHz workstation every point on the graph requires some 17 h and 184 h of computational time for the chains of  $N = 20$  and  $N = 100$  monomers, respectively.

*shifted* to larger values for JNSs, in comparison to the sphere. For PE-sphere adsorption, the change in scaling occurs at  $(\kappa a) \sim 1$ , i.e., when the Debye screening length is comparable to the sphere size  $a$ , in agreement with the theory (see Fig. 1 in Ref. [53]) and the experimental data shown in Fig. 6 in Ref. [64] as well as Fig. 11 in Ref. [51].

The theoretically predicted dependence  $\delta_c(\kappa a)$  for the PE-sphere adsorption [53] given by Eq. (B5) and multiplied by a factor of 1.77 is shown as the solid black curve in Fig. 8B. This numerical factor of the order of unity apparently accounts for all the discrepancies of current simulations performed for finite electrostatically-persistent

PE chains versus the infinitely long unperturbed Gaussian polymers considered in the theory. The agreement with the simulations data both in terms of the magnitude of the critical surface charge density and in terms of the region in which the transition from the cubic to linear scaling in  $\sigma_c(\kappa a)$  occurs, is remarkably good: the theory agrees with the simulations over the range of more than two decades of the sphere size. It is important to note that  $\delta_c$  contains the effects of a finite PE persistence and other chain length effects. For this fact the agreement of the theory [53] with our current simulational results for relatively short chains ( $N = 20$  for the solid symbols in Fig. 8B) is even more remarkable. This observation is a further support for the quantitative validity of the simulations results for PE-JNS adsorption while no theory for this case has been developed to date.

To calculate the error bars for  $\sigma_c$ , we performed a dozen of simulations with different random number seed to generate different sets of chain configurations. For the most data points in Fig. 8 for  $N = 20$  chains the deviation in the critical adsorption conditions is just  $\sim 0.1 \dots 1\%$  of the  $\sigma_c$  value. The error bars are thus much smaller than the symbol size. For longer  $N = 100$  chains the deviations are expectedly larger, namely  $\sim 5 \dots 10\%$  of  $\sigma_c$ . The error bars are of the order of symbol size, except for the first couple of points at the smallest solution salinities, when the error bars can be twice the symbol size. This is physically understandable because in the low-salinity regime, close to the complete desorption threshold, the fluctuations of the polymer dimensions are particularly large. For the others quantities we presented, such as the radius of gyration of the chain  $R_g$  or the width of the adsorbed PE layer  $w$ , the error bars are smaller than symbol size.

## 2. Varying salt concentration

We now turn to the description of the results obtained when the salinity of the solution is changed in the simulations, as shown in Fig. 8A. For a constant radius  $a$ , the PE chain in front of the uniformly charged sphere exhibits the scaling  $\sigma_c \sim (\kappa a)^{1.9}$  in the limit of  $\kappa a \gg 1$  and the scaling  $\sigma_c \sim (\kappa a)^{0.7}$  for  $\kappa a \ll 1$ , in a drastic contrast to Fig. 8B where the particle size was varied. The scaling exponent  $\nu \approx 1.9$  in the limit of  $\kappa a \gg 1$ , which is smaller by about unity than that in the setup with constant salt concentration, is consistent with the effect of the ES PE persistence length  $l_p^{ES}$  on the critical adsorption conditions. This effect is neglected in the simplistic adsorption theory of flexible Gaussian chains [14] for which the scaling  $\sigma_c \sim (\kappa a)^3$  is effected, as prescribed by Eq. (2). For flexible PEs the scaling

$$l_p^{ES}(\kappa) \sim \kappa^\mu \text{ with } \mu \approx -1 \quad (9)$$

is known to hold. According to Eq. (1) and with the total PE persistence length  $l_p = b/2 = l_p^0 + l_p^{ES}$ , the renormalised  $\sigma_c \sim (\kappa a)^2$  scaling for  $\kappa a \gg 1$  is obtained

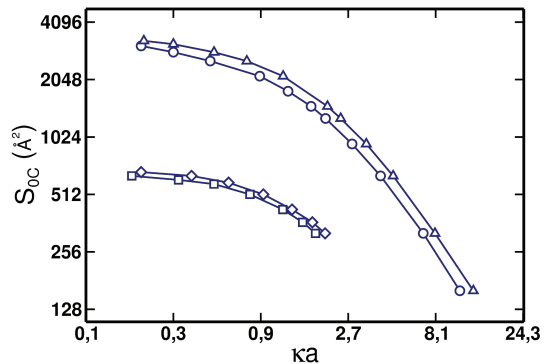


Figure 9: Critical area  $S_0 = e_0/|\sigma_c|$  per surface charge on a Janus particle for PE-JNS adsorption as function of the surface curvature and the salinity. The results are obtained with the exact ES potential  $\Psi_J(r, \theta)$  (circles and squares) and the  $l = 0, 1$  terms in Eq. (A3) (triangles and rhombi symbols). The solution salinity is varied while the other parameters are  $N = 20$ ,  $a = 70$  Å (upper curves) and  $a = 30$  Å (lower curves).

for the critical adsorption of PEs with such a  $\kappa$ -dependent persistence length onto a spherical particle, as we indeed observe in the simulations when  $\kappa$  is varied.

In the limit  $\kappa a \ll 1$  the scaling exponent in the setup with a varying salt concentration is also somewhat reduced for the sphere, namely down to  $\nu \approx 0.7$ , see the filled symbols in Fig. 8A. For small  $\kappa a$ , overall much smaller values of  $\sigma$  are required to trigger the PE adsorption onto a sphere, as compared to JNSs. This is due to the stronger PE-sphere attraction which overcomes the entropic penalty of the polymer confinement near the adsorbing surface. For the PE-adsorption onto a JNS at varying  $\kappa$  the overall growth of  $\sigma_c$  with  $\kappa a$  at  $\kappa a \ll 1$  is much weaker than for the sphere, as demonstrated by the open symbols in Fig. 8A. For  $\kappa a \ll 1$  the critical surface charge density for PE-JNSs adsorption almost saturates, that is,  $\sigma_c \sim \kappa^\nu$  with  $\nu \ll 1$ . With the adsorption criterion used here we do not observe any increase of the value of  $\sigma_c$  at very small  $\kappa a$ , but we cannot exclude this for modified/different adsorption conventions.

Also note that in the full nonlinear ES model of Eq. (A8) lower ES potentials will occur near the charged interfaces for the same  $\sigma$ , as compared to the linear ES theory of Eq. (A2). Then, to ensure the same PE-surface affinity (8), effectively higher surface charge densities will be necessary. This will serve as another source for a potential increase of  $\sigma_c$  for realistic Janus particles at very low salt conditions, where the nonlinear ES model has to be applied.

Moreover, with the chosen adsorption criterion, longer PE chains which are attracted stronger to the particle surface need weaker Janus hemisphere charge densities  $\sigma_c$  for the adsorption to occur, compare the open squares ( $N = 20$ ) and circles ( $N = 100$ ) in Fig. 8A. This trend is similar to that for PE-sphere adsorption for varying



polymerisation degree of the PE chain, compare Fig. 5 of Ref. [57].

Finally, note that for the critical adsorption conditions presented in Fig. 8 we implemented the full exact ES potential (A3). To save simulation time, it is also possible to use just the first two terms in the ES potential expansion (A3). The obtained results are quite close to the exact ones, over a broad range of parameters, see Fig. 9. In this figure we present the critical surface area  $S_0$  per charge that is a directly measurable experimental parameter:  $S_{0,c} = e_0/|\sigma_c|$ .

## V. DISCUSSION AND CONCLUSIONS

Let us first summarise our main findings. From extensive computer simulations we uncovered the properties of adsorption of flexible PE chains onto net-neutral Janus nanospheres with oppositely charged hemispheres. The adsorbing PE chain occupies the JNS hemisphere of the opposite charge and avoids the like-charged hemisphere of the JNS. We examined the behaviour of the critical adsorption conditions in dependence of the particle surface charge density, the surface curvature, and the length of the PE chain. The latter dependence is particularly hard to predict theoretically. We demonstrated that the PE-JNS adsorption-desorption transition differs in many respects from PE adsorption onto the uniformly charged sphere.

In particular, we discovered that there exists *no* universal parameter  $\kappa a$  that couples the surface curvature and the salinity of the solution. The results for the critical PE-JNS adsorption conditions differ substantially if one separately varies the salt concentration or the JNS radius, as shown in Fig. 8. We rationalised the differences in these scalings using the concept of a salt-dependent PE persistence. We also found that shorter PE chains necessitate larger charge densities on the JNS hemispheres to trigger adsorption. We explored how the width of the adsorbed PE layer is reduced for JNSs with progressively larger surface charge densities, due to stronger ES adsorption. For JNSs the critical surface charge density and the thickness of adsorbed layer throughout remain larger than for the PE adsorption onto uniformly charged spherical particles of the same size and nominal surface charge. This reflects the influence of the JNS hemisphere of the same charge as the PE chain, which opposes the adsorption via repulsive ES JNS-PE interactions.

A direct biological application of our results for PE-JNS interaction is the description of the critical adsorption conditions of flexible and semi-flexible PE chains onto oppositely charged interfaces of spherical and cylindrical geometry that have been thoroughly studied in the lab of Paul Dubin [62–65, 67, 69, 70]. Flexible PE chains in the experiments (such as PAMPS, polyacrylic acid PAA, random copolymers of 2-(acrylamido)-2-methylpropane-sulfonate and acrylamide P(AMPS-AAm), sulfonated poly(vinyl alco-

hol) PVAS, sodium-poly(styrene sulfonate) NaPSS, or poly(dimethyldiallylammonium chloride) PDADMAC) usually have persistence lengths of the order of  $l_p \approx 1 \dots 4$  nm, whereas for semiflexible chains such as double stranded DNA the persistence length is of the order of  $l_p \sim 50$  nm. The oppositely charged surfaces often include dodecyltrimethylamine oxide DMDAO cationic uniformly charged micelles with well titration-controlled surface charge density, controllable dimensions, and a geometry which depends on the salt conditions (spherical micelles occur at low salt and cylindrical ones at high salt conditions). Other complexes include spherical colloidal particles, dendrimers of varying generations, and globular proteins [63] that are often non-homogeneously charged (e.g., BSA bovin serum albumin and lysozyme).

In brief, experimentally the complexation of PEs with oppositely charged particles is measured via the changes in the solution turbidity. The latter is intimately coupled to coacervation, aggregation, and precipitation of complexes. The onset on complex formation is well controlled and precisely measured. Turbidimetric measurements systematically reveal that with increasing solution salinity the critical surface charge density  $\sigma_c$  of the particle surface grows, as seen from Eq. (5). The complex formation of flexible PVAS polymers with nearly uniformly charged DMDAO micelles yields scaling exponents of  $\nu \approx 1.0$  and  $\nu \approx 1.8$  for spherical and cylindrical cases, respectively [64]. For P(AMPS-AAm) complexes with DMDAO micelles the powers are  $\nu \approx 1.4$  and  $\nu \approx 2.5$  [64]. DNA complexation with DMDAO micelles of spherical and cylindrical geometry reveals the exponents of  $\nu \approx 1.6$  and  $\nu \approx 1.8$ , respectively [70].

Charge anisotropies of heterogeneously charged proteins such as BSA can even further reduce the scaling dependence of the critical surface charge density for adsorption with  $\kappa$ . Note that for patchy proteins, to compute the effective surface charge density for adsorption  $\sigma_c$ , the net protein charge was divided over the protein surface. Indeed, the complexation of a number of poly-anions (AMPS/AAm, PAA, pectin) with spherical cationic micelles, dodecyltrimethylammonium bromide/Triton X-100 DTAB/TX-100, revealed the following critical exponents for the critical surface charge density  $\sigma_c \sim \kappa^\nu$ : for uniformly charged micelles  $\nu \approx 1.7$  versus  $\nu \approx 0.9$  for pronouncedly heterogeneous charge distribution of BSA proteins. The BSA charge distribution, with a single relatively large cationic patch present at low salt, was additionally shown to evolve into multi-patchy structure at higher salinities, see Fig. 10 and the original Fig. 11 in Ref. [68].

Thus, at low salinities the anionic part of the BSA surface impedes the poly-anion adsorption onto the protein surface, repelling it electrostatically from the attractive cationic patch and giving rise to dramatically smaller values of the critical exponent  $\nu$ . These experimental observations therefore very nicely support our predictions for the PE conformations in the proximity of the JNSs in Fig. 1 and the much weaker growth of  $\sigma_c$  with  $\kappa$  for

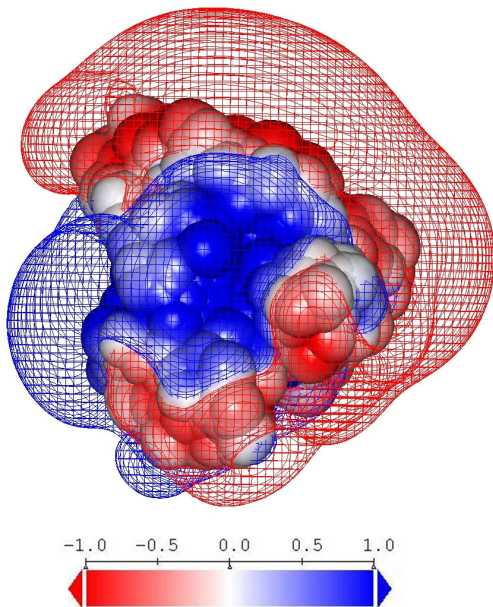


Figure 10: ES potential of the BSA protein, as simulated in Ref. [68] at pH=6.2 and ionic strength of 0.05 M. The blue colour corresponds to a positive potential (a cationic patch). The mesh illustrates the surfaces with the dimensionless potential of  $|e_0\Psi/(k_B T)| = 0.1$ . The red-blue scale denotes the magnitude  $|e_0\Psi/(k_B T)|$  of the potential. The image is from Fig. 11A of Ref. [68], subject to ACS-2006 Copyright. Original figure file courtesy S. Stoll.

PE adsorption onto JNSs, see the results of Fig. 8. The JNSs are somewhat reminiscent in their charge surface pattern to BSA at low salt conditions, as illustrated in Fig. 10. We also note that a number of PE complexes with patchy proteins revealed a maximal affinity as function of the solution salinity realised for Debye screening lengths comparable to the protein dimensions [68].

Another example of PE-protein complexation is the ES-driven wrapping of a negatively charged double-stranded semi-flexible DNA fragment around highly basic histone-core proteins in nucleosome core particles [25]. The latter exhibit an equatorial ring of positive Lysine and Arginine charges [80, 81] forming the strongly non-uniformly charged substrate for the binding of DNA. In both cases, for PE-BSA and DNA-histone adsorption, the surface charge patchiness and structure can give rise to PE adsorption on the *wrong* side of the isoelectric point and to complex overcharging [30] (see, however, also Ref. [82]). One more example of patterned surfaces is the adsorption of DNA onto laterally-structured interfaces of supported cationic lipid membranes, as monitored by atomic force microscopy techniques in Ref. [83], see also Refs. [84] and [85] for, respectively, computer-based and theoretical modelling of DNA complexation with cationic lipid membranes.

In the case of flexible PE-surface adsorption, the ES-driven ordering of flexible single-stranded RNA molecules

on highly positively charged interiors of viral capsids was suggested [86–88]. The RNA adsorption in this system takes place onto strongly non-uniformly charged, patterned surfaces decorated with flexible, highly-basic polypeptide arms. The latter grab the RNAs and trigger mutual complexation, a prerequisite for sustainable thermodynamic self-assembly of single-stranded RNA viruses from the nucleic acid and the protein-subunit components available in the solution [89]. The resulting structure pattern of single-stranded RNA molecules adsorbed to the inner capsid surface obtained both from computer simulations and from experiments indeed resembles the symmetry of viral shells [87].

Extensions of the current simulations scheme will include PE adsorption onto charge-corrugated and patterned Janus surfaces of spherical and cylindrical shape. Also, semiflexible PEs and weak versus strong adsorption conditions will be studied. The latter will e.g. lead to the formation of some ordered, snail-like or toroidal PE structures on oppositely charged caps of the Janus particles, in contrast to the quite disordered PE appearance of flexible chains weakly adsorbed on JNSs, compare Fig. 1. Ordered PE structures, such as tennis-ball like, rosettes, and solenoids, are known to appear in the ground state upon strong PE adsorption onto oppositely and uniformly charged spherical particles, see, e.g., Refs. [21–23, 25, 51]. Lastly, the effects of PE charge heterogeneity and patchiness should be considered in the future, as it is known to affect the critical adsorption conditions as well.

It will be important to test the theoretical results presented here by experimental studies of the different adsorption characteristics of PE chains onto Janus-like nanoparticles, as compared to PE adsorption onto uniformly charged convex surfaces.

## VI. ACKNOWLEDGMENTS

We thank Paul Dubin for insightful comments regarding the PE binding to BSA proteins and to Serge Stoll for kindly providing the original images of the BSA ES surface potential. AGC acknowledges a fruitful collaboration with Roland Winkler over many years. The authors acknowledge financial support from the Academy of Finland (FiDiPro scheme to RM) and the German Research Foundation (DFG grant CH 707/5-1 to ACG). Computer resources were supplied by the Center for Scientific Computing (NCC/GridUNESP) of the São Paulo State University.

### Appendix A: ES potential of the Janus particle

We here derive the ES potential around a JNS. The charge density of a JNS of radius  $a$  with the charge density  $\pm\sigma_0 = \pm e_0/S_0$  on its caps in spherical coordinates

can be written as

$$\sigma(r, \theta) = \sigma_0 \delta(r - a) [\Theta(\pi/2 - \theta) - \Theta(\theta - \pi/2)]. \quad (\text{A1})$$

Here  $\theta$  is the polar angle,  $\Theta(x)$  is the step function,  $e_0 > 0$  is the elementary charge, and  $S_0$  is the area per charge on the surface. The linear Poisson-Boltzmann equation for the ES potential  $\Psi_J$  of a JNS in an electrolyte solution,

$$\nabla_{r,\theta}^2 \Psi_J(r, \theta) = \kappa^2 \Psi_J(r, \theta), \quad (\text{A2})$$

allows the separation of variables via the eigenfunction expansion in terms of Legendre polynomials  $P_l(x)$  and spherical Bessel functions  $K_{l+1/2}(x)$  [51], namely

$$\Psi_J(r, \theta) = \sum_{l=0}^{\infty} C_l P_l(\cos \theta) \frac{K_{l+1/2}(\kappa r)}{\sqrt{\kappa r}}. \quad (\text{A3})$$

Using Gauss' theorem on the particle surface,  $\partial \Psi_J(r, \theta) / \partial r|_{r=a} = -4\pi\sigma(a, \theta)/\epsilon$ , one can restore the distribution of the ES potential, yielding the coefficients of the eigenfunction expansion

$$C_l = \frac{2\pi(2l+1)}{\epsilon k_l(a)} \int_0^\pi P_l(\cos \theta) \sigma(a, \theta) d(\cos \theta), \quad (\text{A4})$$

with  $k_l(a) = [2\kappa a K'_{l+1/2}(\kappa a) - K_{l+1/2}(\kappa a)] / [2a\sqrt{\kappa a}]$  and  $K'(x)$  denoting the derivative. Naturally, the potential  $\Psi_{sp}(r)$  of a uniformly charged sphere is given by the  $l = 0$  term of this expansion, obtained for  $\sigma(r, \theta) = \sigma_0 \delta(r - a)$  as

$$\Psi_{sp}(r) = 4\pi\sigma_0 a^2 \frac{\exp(-\kappa[r-a])}{\epsilon r(1+\kappa a)}. \quad (\text{A5})$$

After integration of  $P_l(x)$ , for a JNS we obtain

$$C_l = -\frac{\sigma_0(2l+1) \left(1 - (-1)^l\right) \pi^{3/2}}{\epsilon k_l(a) \Gamma(1-l/2) \Gamma(3/2+l/2)}, \quad (\text{A6})$$

where  $\Gamma(x)$  is the Gamma function. This yields the ES potential near JNSs used in the simulations. A contour plot of the potential is shown in Fig. 2.

As expected, for JNSs the ES potential shown in Fig. 11 is always lower in magnitude than for a sphere with uniform charge distribution but the same  $\sigma$ . For large JNSs, taking along sufficiently many terms in Eq. (A3), one arrives at the intuitive result that at zero polar angle the asymptotic relation

$$\Psi_J(r, \theta = 0) \rightarrow \Psi_{sp}(r) \quad (\text{A7})$$

hold. The dependence on  $\theta$  illustrated in Fig. 11 shows that close to the “poles” of the JNS the deviation from  $\Psi_{sp}$  is relatively small, while close to the “equator”, i.e., when  $\theta \rightarrow \pi/2$ , the ES potential is strongly diminished by mutual compensation of the ES effect of the two oppositely-charged hemispheres.

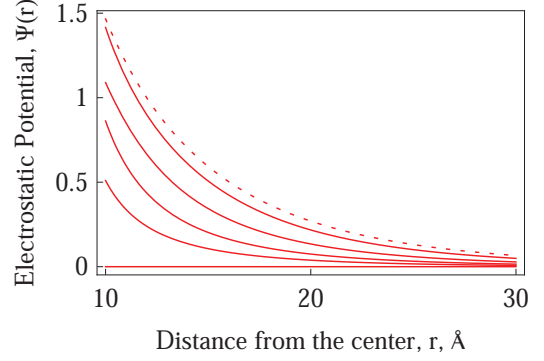


Figure 11: Dimensionless ES potential of a JNS, for polar angles  $\theta = 0, \pi/3, 5\pi/12, 11\pi/24$ , and  $\pi/2$ , for the red solid curves from top to bottom. The dotted curve is the sphere potential  $\Psi_{sp}(r)$  given by Eq. (A5), for identical radius and  $\sigma$ . Parameters are the same as in Fig. 2.

Note here that when we vary the salinity of the solution, it is important to remember that at low salt concentrations the linear Poisson-Boltzmann theory used for the derivation of the potential in Eq. (A3) breaks down due to the high ES potentials near the interface. Therefore, the entire linear ES approach becomes inapplicable in this range. Numerical computations of the ES potential emerging from JNSs in the full non-linear model,

$$\nabla_{r,\theta}^2 \Psi_J(r, \theta) = \kappa^2 \sinh[\Psi_J(r, \theta)], \quad (\text{A8})$$

therefore need to be performed. This is a target for future investigations of more realistic PE-JNS adsorption. We also plan to examine more systematically the effects of the length as well as the linear charge density and the charge patchiness of the PE chain.

## Appendix B: 2D WKB scheme for PE adsorption

We here present the basic equations for the theoretical analysis of the PE-JNS adsorption. Using the WKB method for uniformly charged interfaces established in Ref. [53], one can, in principle, investigate the adsorption of a long PE chain onto a JNS. The equation for the polymer eigenfunctions  $\psi(r, \theta)$  in the external Debye-Hückel potential field  $V_{DH}(r)$  can be derived from the Edwards equation [50]

$$\left( \frac{\partial}{\partial L} - \frac{b}{6} \nabla_{\mathbf{r}}^2 + \frac{V_{DH}(\mathbf{r})}{k_B T} \right) G(\mathbf{r}, \mathbf{r}'; L) = \delta(\mathbf{r} - \mathbf{r}') \delta(L), \quad (\text{B1})$$

written for the polymer's Green function, expanded in terms of eigenfunctions

$$G(\mathbf{r}, \mathbf{r}'; L) = \sum_n \psi_n^*(\mathbf{r}') \psi_n(\mathbf{r}) e^{\mu_n L}. \quad (\text{B2})$$

For polymer chains much longer than the Kuhn length,  $L \gg b$ , the ground state eigenfunction  $\psi_0(e, \theta)$  dominates this expression. With the separation of variables  $\psi_0(r, \theta) = \sum_j \widetilde{R}_j(r) r^{-1} T_j(\theta)$ , because of the linearity of Eq. (B1) for each  $j$  one finds

$$-\mu T_j(\theta) \frac{\widetilde{R}_j(r)}{r} = -\frac{|\rho \Psi_J(r, \theta)|}{k_B T} T_j(\theta) \frac{\widetilde{R}_j(r)}{r} - \frac{b}{6} \left\{ T_j(\theta) \frac{\partial^2 \widetilde{R}_j(r)}{r \partial r^2} + \frac{\widetilde{R}_j(r)}{r^3} \left( \frac{\partial^2 T_j(\theta)}{\partial \theta^2} + \cot \theta \frac{\partial T_j(\theta)}{\partial \theta} \right) \right\} \quad (\text{B3})$$

For a uniformly charged sphere,  $T_j(\theta) \equiv 0$ , and for the radial component we get

$$-\frac{b}{6} \frac{\partial^2 \widetilde{R}_j(r)}{\partial r^2} \frac{1}{r} - \frac{4\pi |\rho \sigma|}{\epsilon k_B T} a^2 \frac{\widetilde{R}_j(r)}{r} \frac{e^{-\kappa(r-a)}}{r(1+\kappa a)} = -\mu \frac{\widetilde{R}_j(r)}{r}. \quad (\text{B4})$$

This equation was solved by the WKB method [53], with the critical adsorption condition as function of the universal parameter  $\kappa a$ ,

$$\delta_c^{sp}(\kappa a) = \frac{6\kappa a(1+\kappa a)C^2}{2\pi e^{\kappa a} \text{erfc}^2(\sqrt{\kappa a/2})}, \quad (\text{B5})$$

where  $\text{erfc}(x) = 1 - \text{erf}(x)$  is the complementary error function and  $C \approx 0.973$ . In the limit  $\kappa a \ll 1$  this leads to Eq. (3) in the main text.

The ES potential  $\Psi_J(r, \theta)$  of a JNS is a sum of coupled radial and polar angle terms, the first term reading  $C_1 \cos \theta K_{3/2}(\kappa r) / \sqrt{\kappa r}$ . The variables for polymer eigenfunctions in the  $(r, \theta)$ -coupled ES field near the JNS cannot be separated, however. Thus, instead of finding an approximate solution of Eq. (B3), in the main text we study the PE-JNS adsorption directly and explicitly by computer simulations. We exploit the critical adsorption conditions and the effect of the *PE length*, which cannot be envisaged from the ground-state-based analysis typically performed for the eigenfunction (B4), which is only applicable to long polymers.

We note that other standard approximations to PE adsorption problems are discussed in Sec. IV of Ref. [56]. We do not consider the charge regulation and self-consistent charge normalisation effects that might affect the PE adsorption properties which was experimentally noticed [90]. No account is taken of changes in the counterion atmosphere upon PE-particle adsorption and a possible low-dielectric JNS interior, see, e.g., Ref. [24] for more on these effects for the standard PE-plane adsorption. Non-ES interactions are not taken into account, see, e.g., Ref. [58] for more details.

- 
- [1] P. G. de Gennes, Rev. Mod. Phys. **64**, 645 (1992).
  - [2] A. Walther and A. H. E. Mueller, Soft Matter **4**, 663 (2008).
  - [3] L. Hong, A. Cacciuto, E. Luijten, and S. Granick, Langmuir **24**, 621 (2008).
  - [4] J. de Graaf, N. Boon, M. Dijkstra, and R. van Roij, J. Chem. Phys. **137**, 104910 (2012).
  - [5] S. Granick, S. Jiang, and Q. Chen, Physics Today **62**, 68 (2009).
  - [6] S. Jiang and et al., Adv. Mater. **4**, 1060 (2010).
  - [7] N. Glaser and et al., Langmuir **22**, 5227 (2006).
  - [8] Y. Chen, Macromolecules **45**, 2619 (2012).
  - [9] J. Du and R. K. O'Reilly, Chem. Soc. Rev. **40**, 2402 (2011).
  - [10] M. Tagliazucchi and I. Szleifer, Soft Matter **8**, 7292 (2012).
  - [11] S. Berger and et al., Macromolecules **41**, 9669 (2008).
  - [12] A. Walther, K. Matussek, and A. H. E. Muller, ACS Nano **2**, 1167 (2008).
  - [13] N. Glaser, D. J. Adams, A. Boeker, and G. Krausch, Langmuir **22**, 5227 (2006).
  - [14] R. G. Winkler and A. G. Cherstvy, Adv. Polym. Sci. **255**, 1 (2014).
  - [15] G. S. Manning, Q. Rev. Biophys. **11**, 179 (1978).
  - [16] G. S. Manning, Macromolecules **40**, 8071 (2007).
  - [17] R. R. Netz and D. Andelman, Phys. Rep. **380**, 1 (2003).
  - [18] A. V. Dobrynin and M. Rubinstein, Prog. Polym. Sci. **30**, 1049 (2005).
  - [19] A. V. Dobrynin, Curr. Opin. Coll. Interf. Sci. **13**, 376 (2008).
  - [20] A. Shafir and D. Andelman, Phys. Rev. E **70**, 061804 (2004).
  - [21] H. Boroudjerdi and R. R. Netz, J. Phys.: Cond. Matt. **17**, S1137 (2005).
  - [22] R. R. Netz and J. F. Joanny, Macromolecules **32**, 9013 (1999).
  - [23] J. Rudnick, R. Bruinsma, and W. M. Gelbart, EPL **51**, 237 (2000).
  - [24] P. Sens and J. F. Joanny, Phys. Rev. Lett. **84**, 4862 (2000).
  - [25] H. Schiessel, J. Phys.: Cond. Matt. **15**, R699 (2003).
  - [26] R. Messina, J. Phys.: Cond. Matt. **21**, 113102 (2009).
  - [27] R. de Vries and M. Cohen-Stuart, Curr. Opin. Coll. Interf. Sci. **11**, 295 (2006).
  - [28] R. Podgornik and M. Licer, Curr. Opin. Coll. Interf. Sci. **11**, 273 (2006).
  - [29] I. Szilagyi and et al., Soft Matter **10**, 2479 (2014).
  - [30] H. Boroudjerdi, A. Naji, and R. R. Netz, Europ. Phys. J. E **37**, 21 (2014).
  - [31] J. Shin, A. G. Cherstvy, and R. Metzler, Phys. Rev. X **4**, 021002 (2014).
  - [32] C. Y. Kong and M. Muthukumar, J. Chem. Phys. **109**, 1522 (1998).
  - [33] A. Akinchina and P. Linse, Macromolecules **35**, 5183 (2002).
  - [34] J. M. Y. Carrillo and A. V. Dobrynin, Langmuir **28**, 1531 (2012).
  - [35] B. Nandy and P. K. Maiti, J. Phys. Chem. B **115**, 217 (2011).
  - [36] Q. Cao and M. Bachmann, Soft Matter **9**, 5087 (2013).

- [37] S. C. C. Nunes, T. F. G. G. Cova, and A. A. C. C. Pais, *J. Chem. Phys.* **139**, 054906 (2013).
- [38] J. Faraudo and A. Martin-Molina, *Curr. Opin. Coll. Interf. Sci.* **18**, 517 (2013).
- [39] G. Luque-Caballero, A. Martin-Molina, and M. Quesada-Perez, *J. Chem. Phys.* **140**, 174701 (2014).
- [40] X. Man and D. Yan, *Macromolecules* **43**, 2582 (2010).
- [41] Z. Wang and et al., *Macromolecules* **44**, 8607 (2011).
- [42] H. Huang and E. Ruckenstein, *Langmuir* **28**, 16300 (2012).
- [43] T. A. Kampmann, H. H. Boltz, and J. Kierfeld, *J. Chem. Phys.* **139**, 034903 (2013).
- [44] S. J. de Carvalho and D. L. Z. Caetano, *J. Chem. Phys.* **138**, 244909 (2013).
- [45] F. W. Wiegel, *J. Phys. A: Math. Gen.* **10**, 299 (1977).
- [46] M. Muthukumar, *J. Chem. Phys.* **86**, 86 (1987).
- [47] F. van Goeler and M. Muthukumar, *J. Chem. Phys.* **100**, 7796 (1994).
- [48] A. Baumgaertner and M. Muthukumar, *J. Chem. Phys.* **94**, 4062 (1991).
- [49] R. R. Netz and J. F. Joanny, *Macromolecules* **32**, 9026 (1999).
- [50] R. G. Winkler and A. G. Cherstvy, *Phys. Rev. Lett.* **96**, 066103 (2006).
- [51] A. G. Cherstvy and R. G. Winkler, *J. Chem. Phys.* **125**, 064904 (2006).
- [52] R. G. Winkler and A. G. Cherstvy, *J. Phys. Chem. B* **111**, 8486 (2007).
- [53] A. G. Cherstvy and R. G. Winkler, *Phys. Chem. Chem. Phys.* **13**, 11686 (2011).
- [54] J. Wang and M. Muthukumar, *J. Chem. Phys.* **135**, 194901 (2011).
- [55] A. G. Cherstvy, *Biopolymers* **97**, 311 (2012).
- [56] A. G. Cherstvy and R. G. Winkler, *J. Phys. Chem. B* **116**, 9838 (2012).
- [57] S. J. de Carvalho, *EPL* **92**, 18001 (2010).
- [58] J. Forsman, *Langmuir* **28**, 5138 (2012).
- [59] F. Carnal and S. Stoll, *J. Phys. Chem. B* **115**, 12007 (2011).
- [60] S. Ulrich, M. Seijo, F. Carnal, and S. Stoll, *Macromolecules* **44**, 1661 (2011).
- [61] S. Ulrich, A. Laguerre, and S. Stoll, *Macromolecules* **115**, 8939 (2005).
- [62] K. Chen and et al., *Biomacromolecules* **12**, 2552 (2011).
- [63] A. B. Kayitmazer and et. al., *Soft Matter* **9**, 2553 (2013).
- [64] X. H. Feng and et. al., *Macromolecules* **34**, 6373 (2001).
- [65] D. W. McQuigg, J. L. Kaplan, and P. L. Dubin, *J. Phys. Chem.* **96**, 1973 (1992).
- [66] M. Antonov, M. Mazzawi, and P. L. Dubin, *Biomacromolecules* **11**, 51 (2010).
- [67] C. L. Cooper, P. L. Dubin, A. B. Kayitmazer, and S. Turksen, *Curr. Opin. Coll. Interf. Sci.* **10**, 52 (2005).
- [68] C. L. Cooper and et al., *Biomacromolecules* **7**, 1025 (2006).
- [69] E. Kizilay and et. al., *Adv. Coll. Interf. Sci.* **167**, 24 (2011).
- [70] Y. Wang, P. L. Dubin, and H. Zhang, *Langmuir* **17**, 1670 (2001).
- [71] J. McNamara, C. Y. Kong, and M. Muthukumar, *J. Chem. Phys.* **117**, 5354 (2002).
- [72] N. Hoda and S. Kumar, *J. Chem. Phys.* **128**, 124907 (2008).
- [73] M. Muthukumar, *J. Chem. Phys.* **103**, 4723 (1995).
- [74] M. Ellis, C. Y. Kong, and M. Muthukumar, *J. Chem. Phys.* **112**, 8723 (2000).
- [75] R. de Vries and et. al., *J. Chem. Phys.* **118**, 4649 (2008).
- [76] R. S. Dias and et. al., *J. Phys. Chem. B* **109**, 11781 (2005).
- [77] Note that the applicability of the variational Ansatz [73] might be questionable in some cases. For instance, it predicts a quadratic  $\sigma_c(\kappa)$ -scaling for PE-cylinder adsorption, failing however to recover the linear  $\sigma_c(\kappa)$  law for PE-sphere adsorption, as derived by the WKB method [53]. Note also that the form of optimized variational functions might differ for various geometries or for patterned surfaces.
- [78] R. de Vries, *J. Chem. Phys.* **120**, 3475 (2004).
- [79] F. Carlsson, P. Linse, and M. Malmsten, *J. Phys. Chem. B* **105**, 9040 (2001).
- [80] K. Luger and et. al., *Nature* **389**, 251 (1997).
- [81] A. G. Cherstvy, *J. Phys. Chem. B* **113**, 4242 (2009).
- [82] A. A. Zinchenko, K. Yoshikawa, and D. Baigl, *Phys. Rev. Lett.* **95**, 228101 (2005).
- [83] H. Clausen-Schaumann and H. E. Gaub, *Langmuir* **15**, 8246 (1999).
- [84] O. Farago, N. Gronbeck-Jensen, and P. Pincus, *Phys. Rev. Lett.* **96**, 018102 (2006).
- [85] A. G. Cherstvy and E. P. Petrov, *Phys. Chem. Chem. Phys.* **16**, 2020 (2014).
- [86] V. A. Belyi and M. Muthukumar, *Proc. Natl. Acad. Sci. U.S.A.* **103**, 17174 (2006).
- [87] C. Forrey and M. Muthukumar, *J. Chem. Phys.* **131**, 105101 (2009).
- [88] A. Siber, A. L. Bozic, and R. Podgornik, *Phys. Chem. Chem. Phys.* **14**, 3746 (2012).
- [89] J. D. Perlmutter, C. Qiao, and M. F. Hagan, *eLife* **2**, e00632 (2013).
- [90] Y. P. Wen and P. L. Dubin, *Macromolecules* **30**, 7856 (1997).